A General Model for the Longevity of Super-Hydrophobic Surfaces in Under-Saturated, Stationary Liquid

Aleksey Bourgoun
Department of Mechanical Engineering,
University of Massachusetts Dartmouth,
Dartmouth, MA 02747
e-mail: abourgoun@umassd.edu

Hangjian Ling[1]
Department of Mechanical Engineering,
University of Massachusetts Dartmouth,
Dartmouth, MA 02747
e-mail: hling1@umassd.edu

We perform a numerical study of the longevity of a super-hydrophobic surface (SHS) in under-saturated, stationary liquid. We numerically solve the spatial-temporal evolution of the gas concentration in the liquid, the time-variation of mass flux of gas out of the plastron, as well as the time required for the gas in the plastron to be fully dissolved (i.e., the plastron lifetime). We find that the profiles of gas concentration at different times are self-similar, and the mass flux reduces with time (t) at a rate of $1/t^{0.5}$. In addition, we examine the impact of texture parameters, including pitch, gas fraction, texture height, and advancing contact angle, on the diffusion process. Our results show that both plastron lifetime and diffusion length increase with increasing the gas fraction or increasing the texture height and are independent of the advancing contact angle and pitch. We propose simple analytical models for plastron lifetime and diffusion length. We show that the model has a fair agreement with the experimental data reported in the literature, and can predict the longevity for SHS with various texture geometries, texture sizes, and under different degrees of under-saturations. Our models could guide the design of long-life SHS for underwater applications such as reducing skin-friction drag and preventing biofouling. [DOI: 10.1115/1.4053678]

1 Introduction

The super-hydrophobic surface (SHS) has received growing attention in recent years due to its potential for wide engineering applications. When submerging in liquid, the SHS can entrap a layer of gas bubbles (or plastrons) between the solid surface and the liquid, forming the so-called Cassie-Baxter state [1]. The gas layer could protect underwater surfaces from corrosion and biofouling [2,3]. Moreover, the gas layer could support a shear-free boundary, resulting in a reduction of skin frictions in both laminar [4–8] and turbulent flows [9–18]. However, implementing the SHS in real engineering systems is still a challenge [19]. One main reason is that the entrapped gas on the SHS could sometimes be replaced by the liquid, leading to a transition from the Cassie-Baxter state to the Wenzel state [20] (i.e., a wetting transition). A wetted SHS loses the most benefits [2,21]. In addition to pressure [22–29] and flow-induced shear stress [30,31], gas dissolution into under-saturated liquid [32,33] is one of the main reasons causing the wetting transition. This study aims to better understand this gas dissolution process, and develop an analytical model to predict the SHS longevity in under-saturated liquid.

Over the past decade, the dissolution of gas from an SHS into the under-saturated liquid has been extensively studied through a combination of numerical, experimental, and analytical approaches. In early numerical studies [34–38], the rate of mass transfer from the plastron to surrounding liquid (i.e., the speed of plastron loss) was modeled by assuming an *invasion coefficient* of gas [39]. As a result, the mass transfer rate was found to be constant during the depinning stage [23] where the interface slides down along the sidewalls with a constant shape. Based on this model, the impacts of liquid pressure [34,36,38] and texture geometry [34,35,38] on the plastron longevity were investigated. Later, Kadoko et al. [40] calculated the rate of mass transfer analytically by approximating the gas dissolution problem in one dimension and solving the dissolved gas concentration in the liquid. Different from the previous numerical studies, Kadoko et al. found that the mass transfer rate reduces during the depinning stage. They examined the plastron longevity as a function of texture height and initial gas concentration in the liquid.

In the experimental studies, the wetting transition induced by the gas dissolution has been observed through various optical techniques, such as Total-Internal-Reflection [41–44], Confocal Microscopy [45–47], X-Ray Diffraction [48], and direct imaging [49,50]. The plastron longevity was measured either directly by tracking the movement of the gas–liquid interface [45] or indirectly based on the intensity of the light reflected from the surface [41]. Longevity for SHSs with both regular and irregular texture geometries has been investigated. Most experimental data showed that the plastron longevity decreases with increasing the hydrostatic pressure [43–45] or reducing the dissolved gas in the liquid [50] (in both cases, the degree of liquid under-saturation increases). For low hydrostatic pressures and small texture size, an equilibrium state with zero mass flux can be achieved [49,51].

Analytical models of plastron longevity, which require a preknowledge of diffusion length or invasion coefficient, have been proposed. For example, Lv et al. [45] proposed a characteristic time t_D for an SHS with regular pores in under-saturated liquid

$$t_D = [c_0/(c_0 - c_\infty)] \times h L_D/D_G \tag{1}$$

where h is the height of the texture, L_D is the diffusion length, D_G is the diffusion coefficient, c_0 and c_∞ are the initial gas concentration in the plastron and in the liquid, respectively. By fitting the experimental data, Lv et al. Reported $L_D = 450\,\mu$m. They showed that when normalizing the time by t_D, the movements of the gas–liquid interface under different pressures collapse. Recently, Kim and Park [52] reported a much smaller diffusion length $L_D = 4$ to $6\,\mu$m for a different SHS, suggesting that L_D may vary with texture geometry and liquid pressure. By assuming a known

[1]Corresponding author.

Contributed by the Heat Transfer Division of ASME for publication in the Journal of Heat Transfer. Manuscript received November 11, 2021; final manuscript received January 11, 2022; published online February 10, 2022. Assoc. Editor: Evelyn Wang.

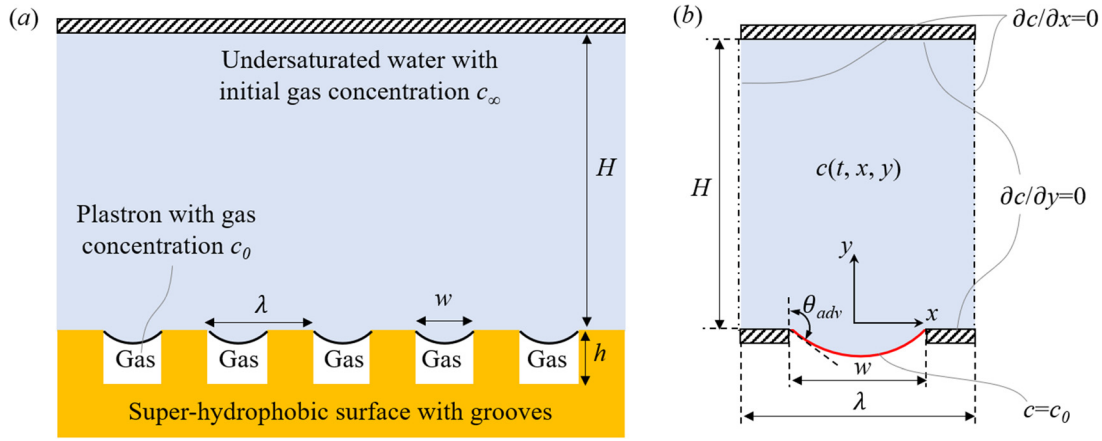

Fig. 1 (*a*) Schematic of a grooved super-hydrophobic surface submerged in under-saturated liquid and (*b*) a simplified model of gas transfer from a plastron to the liquid

invasion coefficient, Hemeda and Tafreshi [38] derived equations of the plastron longevity in two regimes, defined by pressure smaller or larger than the critical pressure for interface to depin from the edge of the texture.

The acceleration of the gas dissolution by external flows has also been studied intensively. For example, by using alternate shear-free and no-slip boundaries [53,54] or a wall with a prescribed slip coefficient [55], several researchers numerically solved the coupled mass and momentum transport equations in laminar flows over SHS. By using an approximate integral method, Barth et al. [56,57] developed first-principles models of the convective gas dissolution in laminar and turbulent flows over SHS. In experimental studies, by measuring the total-internal-reflection light from the SHS, several researchers [58–61] reported a reduction of plastron longevity with increasing *Reynolds number*. By using fluorescence microscopy [53], the spatial distributions of gas concentration were measured in laminar flows over SHS. Recently, by tracking the movement of the gas–liquid interface, scaling laws [52,62,63] of *Sherwood number* were proposed to quantify the convective enhancement of gas dissolution.

Here, we focus on gas dissolution in stationary liquid. We aim to propose a general formula for the plastron longevity, which does not require a per-knowledge of the diffusion length or invasion coefficient. We also aim to propose a model for the diffusion length, which can explain the different values of L_D reported in the literature. To achieve these goals, we numerically solve the spatial and temporal evolutions of the gas concentration in the liquid. The mass transfer rate and plastron lifetime are calculated based on the resolved gas concentration field near the interface. We will show that as gas being slowly dissolved into the liquid, the gas concentration in the liquid increases and the mass transfer rate reduces. In addition, we examine the impacts of texture size, texture shape, and interface shape on plastron longevity. Last, we propose analytical models for the plastron lifetime and diffusion length, which can work for SHS with various texture geometries, texture sizes, and under different degrees of under-saturations.

2 Numerical Methods

2.1 Problem Description. In this study, we focus on the gas transfer from a SHS with microgrooves to the under-saturated liquid, as shown in Fig. 2(*a*). The geometry of the groove is characterized by three parameters, groove pitch λ, groove width w, and groove height h. The SHS is installed on the bottom wall of a closed chamber, which has a height of $H = 100$ mm and is filled with water. The gas trapped in the plastron is air, with a density of $\rho_{gas,0} = 1.2\,kg/m^3$ (evaluated at atmosphere pressure). The diffusion coefficient of the air in the water is $D_G = 2.0 \times 10^{-9}$ m^2/s. The water is initially saturated with air at atmosphere pressure so that $c_\infty = 0.023\,kg/m^3$. The pressure in the water above the SHS is denoted as P_L.

When P_L is equal to the atmosphere pressure, the gas–liquid interface is flat and there is no gas flux. As increasing P_L, the interface becomes curved, c_0 increases, and the gas dissolution takes place when c_0 is larger than c_∞. Depending on whether P_L is larger than the critical pressure for the interface to depin, the wetting transition can experience either a two-stage or a one-stage process [34]. When P_L is smaller than the critical pressure, the wetting process consists of two stages: an initial sagging and a depining impalement. During the first stage of initial sagging, the interface increases its curvature while pinning to the tip of the texture. During the second stage of depining impalement, the interface detaches from the tip of the texture, slides down along the sidewalls of the groove, and maintains a constant shape. The interface depin only after the local contact angle reaches the advancing contact angle θ_{adv}. For SHS with single-length scale texture, θ_{adv} is typically smaller than 120 deg [23,24,45]. For SHS with double-length scale hierarchical texture, θ_{adv} can exceed 120 deg [63–65]. On the other hand, when P_L is larger than the critical pressure, the wetting process only includes the second stage of depining impalement.

In this study, we consider only the depining impalement for simplicity. We set $c_0 = 1.2c_\infty = 0.028\,kg/m^3$, resembling a case with $P_L \approx 1.2$ atm, much larger than the critical pressure for the interface to depin. Although ignoring the initial sagging, our simulations provide an approximation of the plastron lifetime for SHS with larger ratios of groove height to width. As listed in Table 1, we vary the pitch, ratio of groove width to pitch, and ratio of groove height to pitch to study the impact of texture geometry on the gas dissolution. In addition, we vary θ_{adv} from 90 deg to 150 deg to study the impact of surface hydrophobicity and hierarchical texture on gas dissolution.

2.2 Numerical Model. To simulate the gas dissolution process described above, we use a simplified model shown in Fig. 2(*b*). First, we assume that the rate of gas dissolution is identical for different grooves on the SHS. Thus, instead of solving for the entire surface, the model only simulates the gas transfer for a single groove and uses a symmetric boundary condition on the two sides of the domain. This assumption is valid when the surface is much larger than the diffusion length. Second, considering that

Table 1 Values of texture parameters used in the simulations

λ (μm)	w/λ	h/λ	θ_{adv}
50–500	0.1–0.9	0.2–4	90 deg–150 deg

the displacement of the gas–liquid interface is negligible compared to the height of simulation domain, we assume that the interface is fixed in space during the wetting process. To validate this assumption, we performed two simulations where the interface is fixed either at the tip of the groove or at the bottom of the groove. We find that the plastron longevities calculated from the two simulations differ by less than 1%.

We denote x and y as the Cartesian coordinates (y is the direction normal to the surface), and t is the time. We set $y=0$ at the tip of the groove, and $x=0$ at the middle of the groove. The evolution of dissolved gas concentration in the liquid $c(x, y, t)$ is governed by the following equation:

$$\frac{\partial c}{\partial t} = D_G\left(\frac{\partial^2 c}{\partial x^2} + \frac{\partial^2 c}{\partial y^2}\right) \tag{2}$$

The boundary conditions are shown in Fig. 2(*b*). We set no gas flux boundary condition at the top of the domain

$$\frac{\partial c}{\partial y} = 0 \quad \text{on} \quad y = H \tag{3}$$

It should be noted that replacing this Neumann boundary condition to Dirichlet boundary condition, $c(y=H)=c_\infty$, would not change the simulation results. The reason is that the height of the simulation domain is sufficiently large such that at the end of the simulations (i.e., when all the gas in the plastron has been transferred into the liquid), the gas concentration at $y=H$ remains unchanged.

At the bottom of the simulation domain, we set no flux at the solid portion of the SHS and a constant gas concentration c_0 at the gas–liquid interface

$$\frac{\partial c}{\partial y} = 0 \quad \text{on} \quad y = 0, \quad w/2 < |x| < \lambda/2 \tag{4}$$

$$c = c_0 \quad \text{on} \quad \text{gas} - \text{liquid interface} \tag{5}$$

The reason a fixed gas concentration is used at the interface is because the gas pressure in the plastron remains as a constant during the depining impalement.

There is no gas flux on the sides of the simulation domain due to the symmetric boundary condition

$$\frac{\partial c}{\partial x} = 0 \quad \text{on} \quad x = \pm\frac{\lambda}{2} \tag{6}$$

The initial condition is set as

$$c(t=0) = c_\infty \tag{7}$$

After the gas concentration in the liquid is obtained, the average flux of mass transferring out from the plastron into the liquid, denoted as J_{out}, can be calculated by based on the Fick's first law

$$J_{\text{out}}(t) = -\frac{1}{A}\int\int D_G\frac{\partial c}{\partial n}dS \tag{8}$$

where $A=-w(\theta_{\text{adv}}-\pi/2)/\cos\theta_{\text{adv}}$ is the interface area per unit depth into the page, $\partial c/\partial n$ is the gradient of gas concentration normal to the interface, and the integral is evaluated along the interface S. The mass of gas remaining in the plastron (per unit depth into the page), denoted as m, is calculated as

$$m(t) = m_0 - A\int_0^t J_{\text{out}}(t')dt' \tag{9}$$

where $m_0=\rho_{\text{gas},0}wh$ is initial mass of gas in the plastron. We define and calculate the plastron lifetime t_f as the time when m is equal to zero

$$m(t=t_f) = 0 \tag{10}$$

The above-mentioned governing equation with the prescribed boundary and initial conditions is numerically solved in COMSOL Multiphysics 5.4. For simulation domain near the surface ($0<y<5$ mm), a small square element of size $2\,\mu\text{m}\times 2\,\mu\text{m}$ is used. For the domain near the curved interface ($y<0$), a triangle element of size $2\,\mu$m is used. Far away from the surface ($y>5$ mm), a larger element is used. A time interval ranging from 4 to 2500 s is used depending on the plastron lifetime (a larger time interval is selected for cases with a larger plastron lifetime). The number of time-step is about 700. Further reducing element size or time interval does not change the plastron lifetime by more than 3%.

To better understand the gas diffusion process, we calculate the time-average mass flux J_{ave} as

$$J_{\text{ave}} = \frac{m_0}{wt_f} = \frac{D_G(c_o - c_\infty)}{L_D} \tag{11}$$

where L_D is the diffusion length which indicates how far the gas in the plastron propagates into the liquid at the end of wetting process. Solving this equation, the diffusion length can be expressed as

$$L_D = \frac{D_G(c_o - c_\infty)t_f}{\rho_{\text{gas},0}h} \tag{12}$$

Note, Eq. (12) is very similar to the analytical model of characterize time scale proposed by Lv et al. [45] shown in Eq. (1). When the diffusion length is known, the plastron lifetime can be calculated from Eq. (12). We attempt to understand what parameters impact L_D, propose an analytical model for L_D as well as for t_f.

3 Results and Discussion

3.1 A Typical Case. First, we present the simulation results of a typical gas dissolution process for a grooved SHS with $\lambda=100\,\mu$m, $w/\lambda=0.5$, $h/\lambda=1.0$, and $\theta_{\text{adv}}=120$ deg. Figure 3 shows the spatial distributions of gas concentration near the SHS at the early stage of wetting transition. At the very beginning $D_Gt/\lambda^2<10$, only the gas concentration near the gas–liquid interface is impacted, while the gas concentration far away from the plastron is unchanged. As time goes on, the gas from the plastron propagates further into the liquid in both x and y directions, and the gas concentration in the liquid further away from the surface increases. For $D_Gt/\lambda^2>10$, the gas concentration near the surface is nearly uniform along the x-direction. The gas propagation can be approximated in one dimension.

Figure 4(*a*) shows x-averaged gas concentration as a function of y at three different times, $t=0.2$, 0.5, and $0.8t_f$. As expected, the gas concentration changes from c_0 to c_∞ as moving from the surface to the far-field of the liquid. Moreover, as increasing time, the y-gradient of gas concentration reduces, which indicates a reduction of mass transfer rate during the wetting transition. Figure 4(*b*) shows the same profiles in Fig. 4(*a*) plotting as a function of $y/(D_Gt)^{0.5}$. Interestingly, the three profiles collapse and agree well with the analytical solution $1-\text{erf}[y/2(D_Gt)^{0.5}]$. This result implies that the concentration profiles at different times are self-similar and $\partial c/\partial y$ reduces at a rate of $1/t^{0.5}$.

Figure 4(*c*) shows the time-variation of the mass of gas remaining in the plastron. For comparison, we plot the solution by Kadoko et al. [40], who approximated the gas dissolution in one dimension and analytically solved the dissolved gas concentration in the liquid. Kadoko et al. also considered the initial sagging and the change of gas pressure in the plastron. Although our simulation ignored the initial sagging, the trend of mass variation shows a good agreement with their result. As increasing time, the mass in the plastron reduces and reaches to 0 at $t=t_f$. Moreover, as

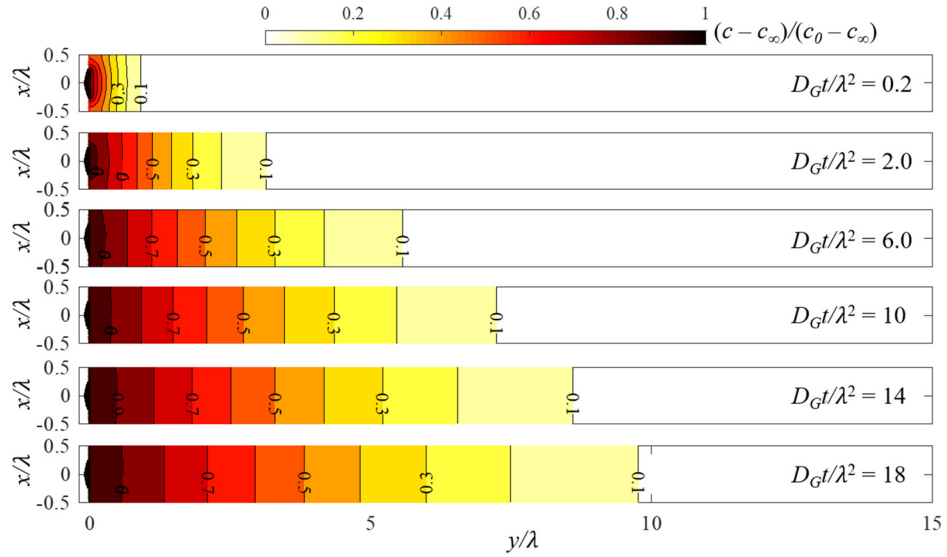

Fig. 2 Spatial distributions of the gas concentration in the liquid near the SHS at the early stage of the wetting process. For the case shown, $\lambda = 100\,\mu$m, $w/\lambda = 0.5$, $h/\lambda = 1$, and $\theta_{adv} = 120$ deg. The gas–liquid interface is located near the origin. To obtain these results, the time interval in set to be 1 s, which is much smaller than the one used to obtain the plastron lifetime.

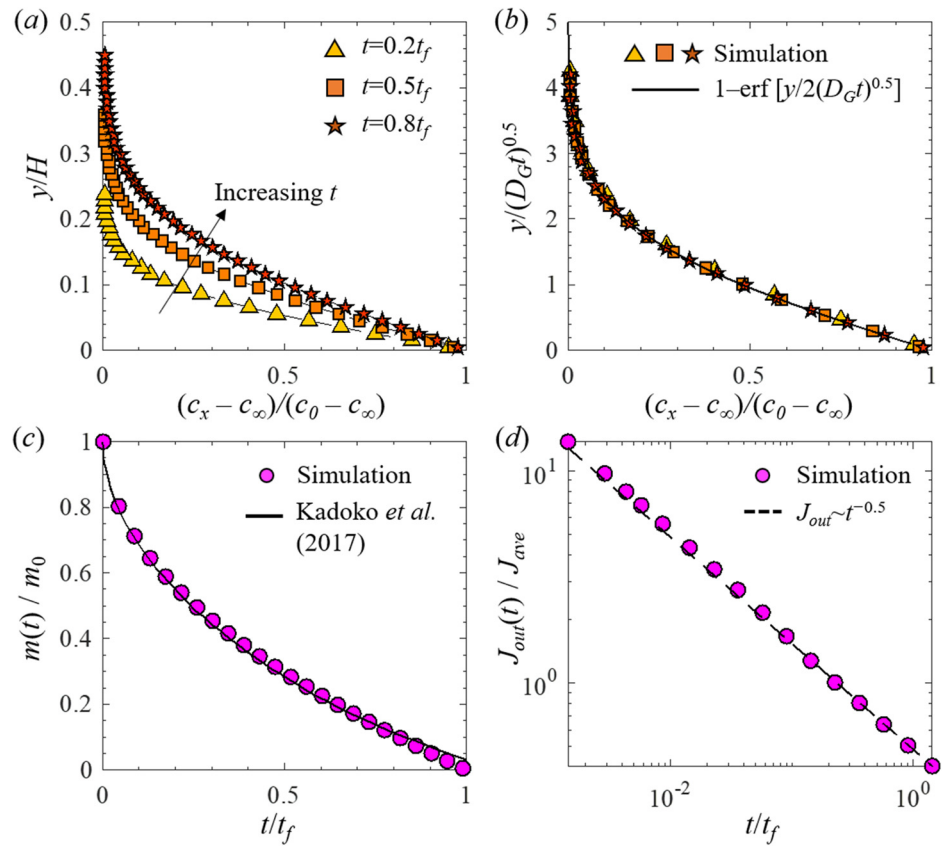

Fig. 3 (*a*)–(*b*) *x*-averaged gas concentration as a function of y/H (*a*) and $y/(D_Gt)^{0.5}$ (*b*) at three selected times $t = 0.2$, 0.5 and 0.8 t_f. (*c*)–(*d*) Time variations of remaining mass of gas in the plastron (*c*) and mass flux of gas out of the plastron (*d*). For the case shown, $\lambda = 100\,\mu$m, $w/\lambda = 0.5$, $h/\lambda = 1$, and $\theta_{adv} = 120$ deg.

increasing time, the rate of mass loss decreases. As shown in Fig. 4(*d*), we find that J_{out} reduces at a rate of $1/t^{0.5}$, which is consistent to the self-similar behavior of the gas concentration profiles. This trend is expected since as increasing time, the gas concentration in the liquid increases, and the gradient of gas concentration near the SHS reduces.

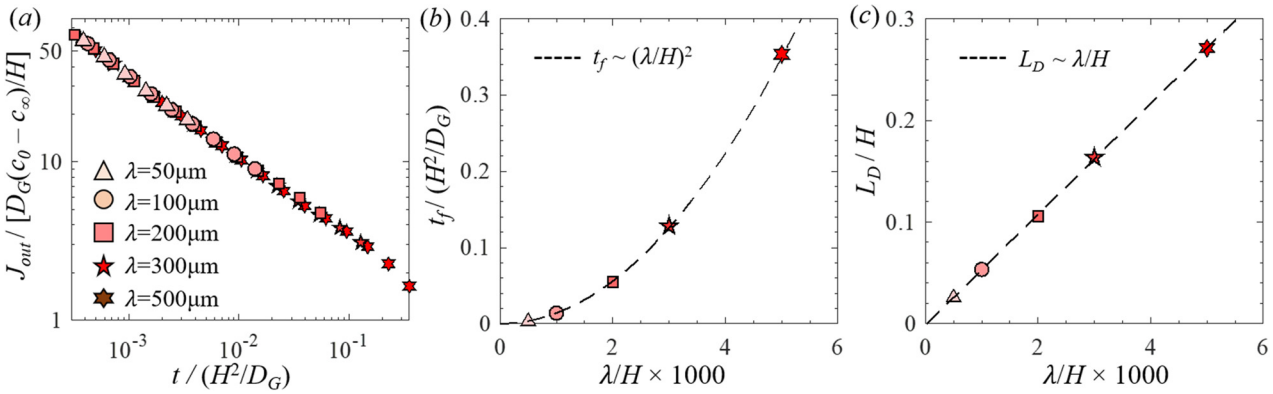

Fig. 4 Impact of texture size on the mass flux out of the plastron (*a*), the lifetime of the plastron (*b*), and the diffusion length (*c*). In these simulations, $w/\lambda = 0.5$, $h/\lambda = 1$, and $\theta_{adv} = 120$ deg.

It should be emphasized that the current result is different from previous numerical studies [34–38] which assumed a constant invasion coefficient and found a constant mass flux during the depining wetting stage. And the current result only applies to cases where the liquid is stationary. When the SHS is exposed to external flows, a concentration boundary layer could be developed over the SHS [53], and the gas concentration in the boundary layer may not vary during the wetting transition.

Based on the above observations, we can assume the following relationship for J_{out}:

$$J_{out} = G\left(\frac{\lambda}{H}, \frac{w}{\lambda}, \frac{h}{\lambda}, \frac{w}{A}\right) \times \frac{D_G{}^{0.5}(c_o - c_\infty)}{t^{0.5}} \tag{13}$$

where G is a nondimensional parameter depending on four texture parameters: λ/H, w/λ, h/λ, and w/A. Here, λ/H denotes the ratio of texture size to domain height, w/λ and h/λ are related to the texture shape, and $w/A = (\cos\theta_{adv})/(\pi/2\text{-}\theta_{adv})$ is the ratio of groove width to interface area depending only on θ_{adv}. For flat interface, $\theta_{adv} = 90$ deg and $w/A = 1$. For curved interface, $\theta_{adv} > 90$ deg and $w/A < 1$. The larger the θ_{adv}, the smaller the w/A. Substituting Eq. (13) into Eqs. (9) and (12), the following two scaling relationships for the plastron lifetime and the diffusion length can be found

$$\frac{D_G t_f}{H^2} \sim \frac{\rho_{gas}^2}{(c_0 - c_\infty)^2} \times G^{-2} \times \left(\frac{w}{A}\right)^2 \times \left(\frac{h}{\lambda}\right)^2 \times \left(\frac{\lambda}{H}\right)^2 \tag{14}$$

$$\frac{L_D}{H} \sim \frac{\rho_{gas}}{(c_0 - c_\infty)} \times G^{-2} \times \left(\frac{w}{A}\right)^2 \times \frac{h}{\lambda} \times \frac{\lambda}{H} \tag{15}$$

Thus, according to Eqs. (14) to (15), the plastron lifetime and diffusion length can be predicted if G is known. In the next sections, we will perform a series of numerical simulations to study the dependencies of G, J_{out}, t_f, and L_D on the four parameters: λ/H, w/λ, h/λ, and θ_{adv}.

3.2 Effects of Texture Parameters on Gas Diffusion. First, we run a series of simulations where λ/H varies, and w/λ, h/λ, and θ_{adv} are fixed. This resembles a situation where SHSs of different texture sizes are submerged in water at fixed depth. Figure 5(*a*) shows the time variations of J_{out} for different λ/H. Interestingly, regardless of λ/H, the profiles of J_{out} for all cases overlap. This result indicates that G is independent of λ/H. Therefore, according to Eqs. (14) and (15), we expect scaling relations: $t_f \sim (\lambda/H)^2$, and $L_D \sim (\lambda/H)$, which are confirmed by Figs. 5(*b*)–5(*c*).

Second, we modify w/λ from 0.1 to 0.9, and fix the values of λ/H, h/λ, and θ_{adv}. This means that the fraction of surface area covered by gas (or the gas fraction ϕ_g) varies. For most SHS, ϕ_g is larger than 0.5. A larger ϕ_g is preferred for drag reduction [27]. Figure 6(*a*) shows the time variations of J_{out} for different w/λ. It is found that with increasing w/λ, J_{out} reduces. This trend is expected since as increasing w/λ, more liquid is exposed to the plastron, the gas concentration in the liquid can adjust more quickly to c_0, and leading to a faster reduction of the normal-gradient of gas concentration. Moreover, as shown in Fig. 6(*b*), the profiles of $J_{out} \times (w/\lambda)$ collapse. It suggests that the J_{out} and G are inversely proportional to the gas fraction, i.e., $J_{out} \sim (w/\lambda)^{-1}$, $G \sim (w/\lambda)^{-1}$. Thus, according to Eqs. (14) and (15), we expect scaling relations: $t_f \sim (w/\lambda)^2$ and $L_D \sim G^{-2} \sim (w/\lambda)^2$, which are confirmed in Figs. 6(*c*)–6(*d*).

Third, we run a number of simulations where h/λ varies from 0.2 to 4, and λ/H, w/λ, and θ_{adv} remain as constants. This means that the texture height varies, while all other parameters are kept same. Figure 7(*a*) shows the time variations of J_{out} for these cases. As shown, the profiles of J_{out} for all cases overlap, indicating that J_{out} and G are independent of h/λ. This result is expected since h is not included in the boundary conditions for solving the dissolved gas concentration in the liquid. As a result, according to Eqs. (14) and (15), we expect scaling relations: $t_f \sim (h/\lambda)^2$ and $L_D \sim h/\lambda$, which are confirmed by Figs. 7(*b*)–7(*c*).

Last, we perform simulations where θ_{adv} varies from 90 deg to 150 deg, and λ/H, w/λ, and h/λ are fixed. Larger θ_{adv} can be obtained by either coating the surface with more hydrophobic materials or adding nanoscale roughness on the side walls of the texture. With increasing θ_{adv}, the interface is more curved, and A/w increases. Figure 8(*a*) shows the time variations of J_{out} for these cases. As shown, J_{out} reduces slightly with increasing θ_{adv}. Similar to increasing w, increasing θ_{adv} effectively increases the contact area between the liquid and plastron. Thus, the liquid can adjust more quickly to c_0, leading to smaller J_{out}. Moreover, as shown in Fig. 8(*b*), when plotting $J_{out} \times (A/w)$, the profiles collapse, indicating that J_{out} and G are linearly proportional to w/A. As a result, the mass transfer rate (AJ_{out}) is same for different θ_{adv}. And according to Eqs. (14) and (15), we expect that t_f and L_D are independent of θ_{adv}, which are confirmed in Figs. 8(*c*)–8(*d*). Although increasing θ_{adv} allows the SHS to sustain higher pressures [22], it may not impact the SHS longevity against gas diffusion.

3.3 Analytical Models of Plastron Lifetime and Diffusion Length. Based on previous numerical simulations, we can conclude that the nondimensional parameter G only depends on w/λ and w/A, and is independent of λ/H and h/λ

$$G\left(\frac{\lambda}{H}, \frac{w}{\lambda}, \frac{h}{\lambda}, \frac{w}{A}\right) \sim \left(\frac{w}{\lambda}\right)^{-1} \times \frac{w}{A} \tag{16}$$

Substituting Eq. (16) into Eqs. (14) and (15), the plastron lifetime and the diffusion length can be modeled as

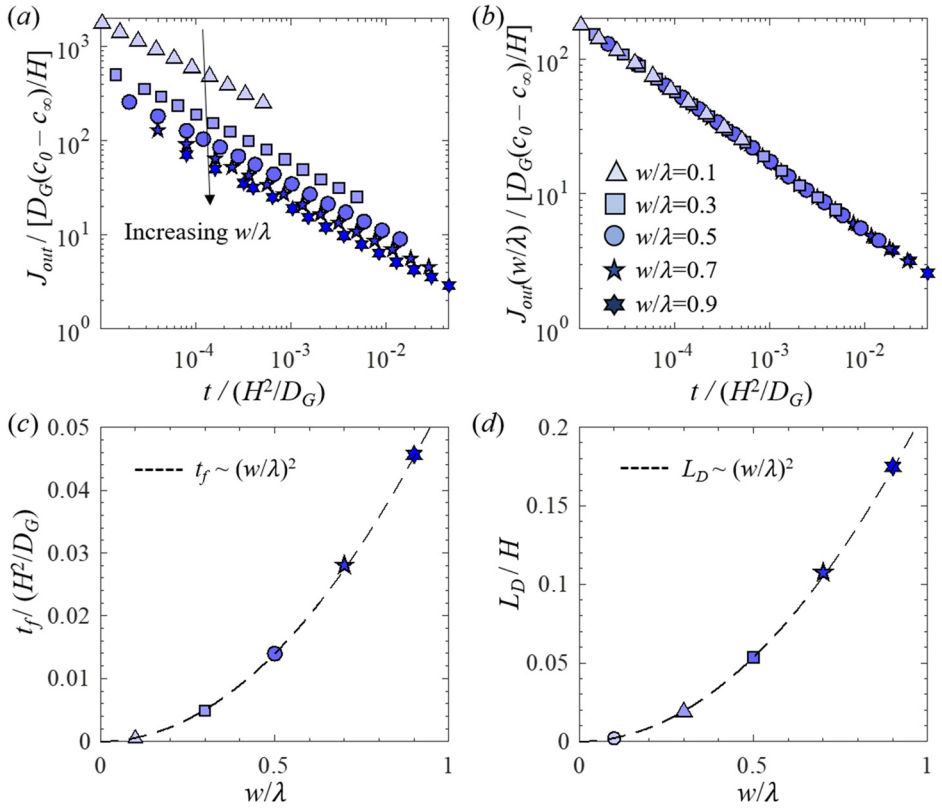

Fig. 5 Impact of ratio of groove width to pitch (w/λ or gas fraction) on the mass flux out of the plastron (*a*)–(*b*), the lifetime of the plastron (*c*), and the diffusion length (*d*). In these simulations, $\lambda = 100\,\mu$m, $h/\lambda = 1$, and $\theta_{adv} = 120$ deg.

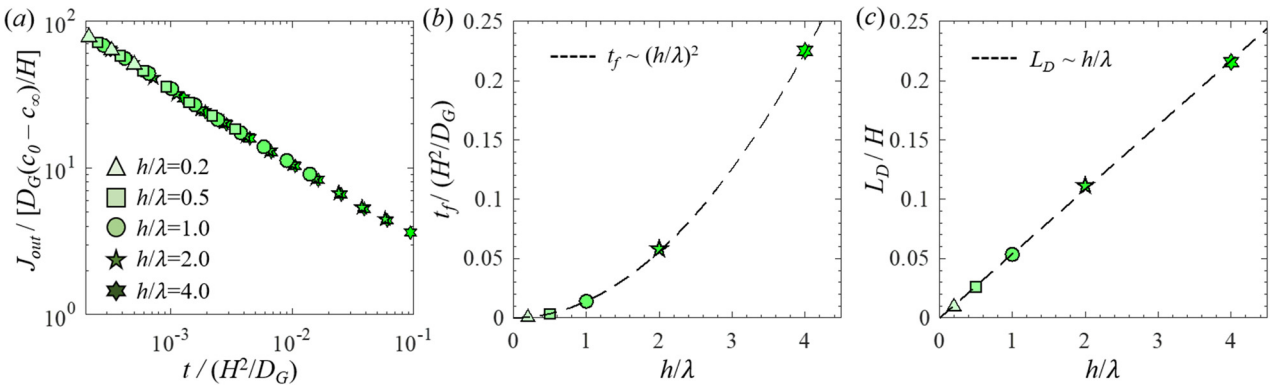

Fig. 6 Impact of ratio of texture height to pitch (h/λ) on the mass flux out of the plastron (*a*), the lifetime of the plastron (*b*), and the diffusion length (*c*). In these simulations, $\lambda = 100\,\mu$m, $w/\lambda = 0.5$, and $\theta_{adv} = 120$ deg.

$$t_f = 0.81 \frac{{\rho_{gas,0}}^2 h^2 \phi_g^2}{D_G (c_0 - c_\infty)^2} \tag{17}$$

$$L_D = 0.81 \frac{\rho_{gas} h \phi_g^2}{(c_0 - c_\infty)} \tag{18}$$

where the constant 0.81 is obtained by fitting the simulation results. We replace w/λ by ϕ_g, since gas fraction is a more general term for characterizing the texture geometry of SHS. As shown in Figs. 9(*a*) and 9(*b*), the plastron lifetimes and diffusion lengths obtained from all simulations in this study can be predicted by Eqs. (17) and (18), although these SHSs have different magnitudes of λ, w, h, and θ_{adv}.

At the limit of $\phi_g \to 1$ and considering a flat interface, the gas diffusion problem can be approximated as one-dimensional (1D), where the gas concentration c^{1D} and the mass flux of gas out of plastron J_{out}^{1D} can be expressed as

$$\frac{c^{1D} - c_\infty}{c_0 - c_\infty} = 1 - \text{erf}\left(\frac{y}{2\sqrt{D_G t}}\right) \tag{19}$$

$$J_{out}^{1D} = D_G \frac{\partial c}{\partial y}|_{y=0} = \frac{1}{\pi^{0.5}} \frac{D_G^{0.5}(c_0 - c_\infty)}{2\sqrt{t}} \tag{20}$$

Substituting Eq. (20) into Eqs. (9) and (12), the plastron lifetime and the diffusion length for the 1D diffusion can be found as

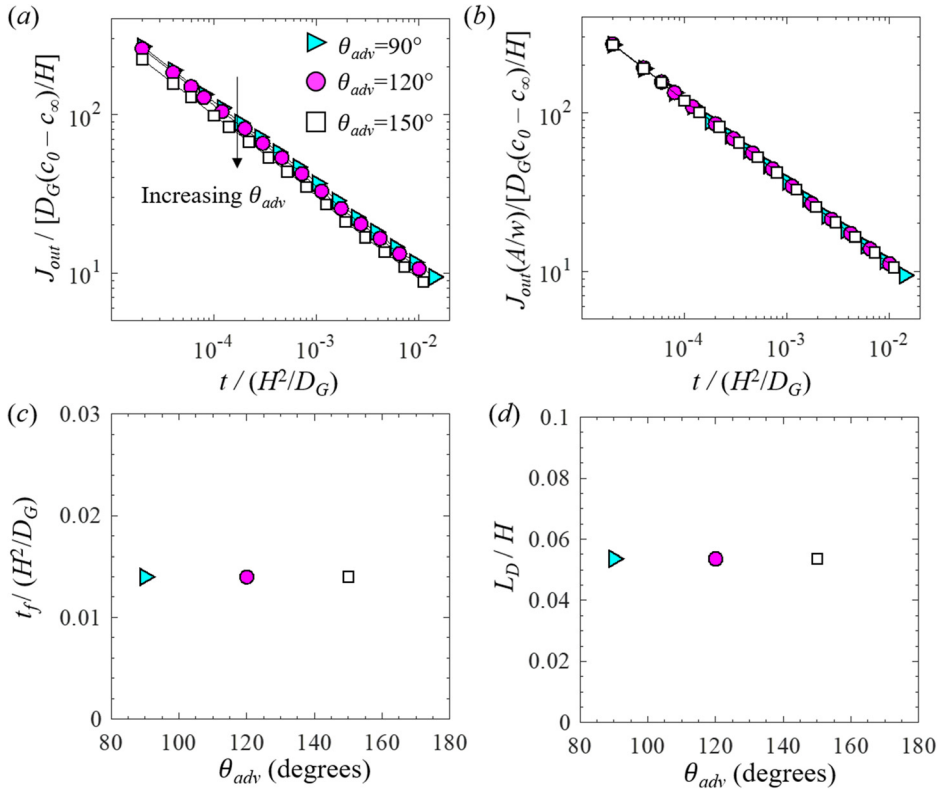

Fig. 7 Impact of the advancing contact angle (θ_{adv}) on the mass flux out of the plastron (*a*)–(*b*), the lifetime of the plastron (*c*), and the diffusion length (*d*). In these simulations, $\lambda = 100\ \mu$m, $w/\lambda = 0.5$, and $h/\lambda = 1$.

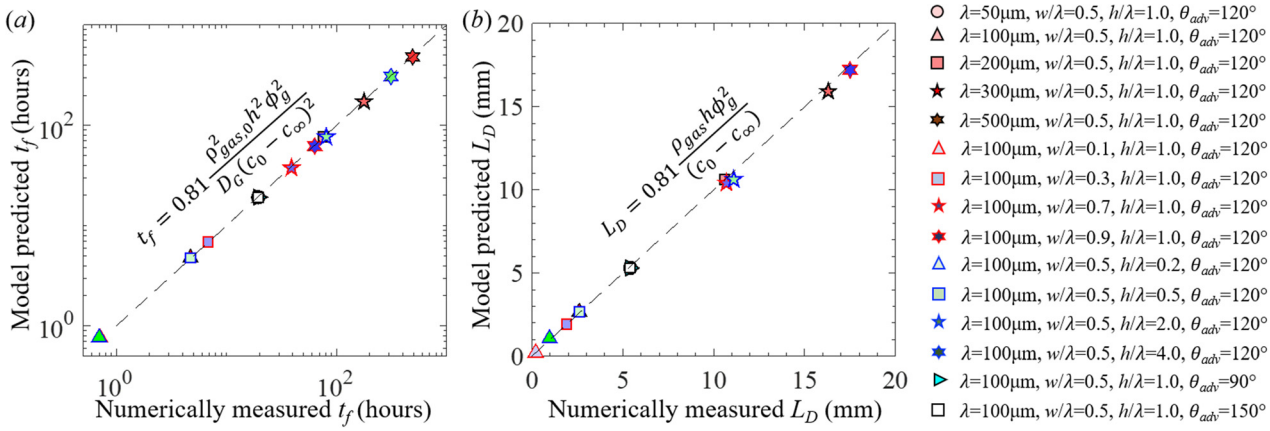

Fig. 8 (*a*) A comparison between numerically measured plastron lifetime and the predicted plastron lifetime and (*b*) a comparison between numerically measured diffusion length and the predicted diffusion length

$$t_f^{1D} = \frac{\pi}{4}\frac{{\rho_{\text{gas},0}}^2 h^2}{D_G(c_0 - c_\infty)^2} \tag{21}$$

$$L_D^{1D} = \frac{\pi}{4}\frac{\rho_{\text{gas}} h}{(c_0 - c_\infty)} \tag{22}$$

Thus, the models of plastron lifetime and diffusion length provided in Eqs. (17) and (18) are very similar to those obtained for 1D diffusion. The only difference is that the models for SHS have an additional term of ${\phi_g}^2$ compared to the models for 1D diffusion where $\phi_g = 1$. The two constants 0.81 and $\pi/4$ differ by less than 5%.

The model provided in Eq. (17) can be readily used to predict the longevity of SHS in under-saturated liquid if the gas fraction, roughness height, and initial gas concentrations in the liquid and plastron are known. A comparison between the experimental measured t_f and model predicted t_f is shown in Fig. 10. The experimental data are taken from five different studies. Since Lv et al. [45] measured the plastron lifetime based on the time when the interface reaches to 0.72 h ($h = 40\ \mu$m for their SHS), we thus use $h = 28.8\ \mu$m in Eq. (17) to estimate t_f. For the randomly roughed SHS used by Hokmabad and Ghaemi [60], we use the reported mean peak to trough height as h, and a gas fraction of 0.6 to 0.9 to estimate the range of t_f. For the randomly roughed SHS studied in Poetes et al. [43], we use the reported plastron thickness of a fresh immersed SHS as h, and a gas fraction of 0.6–0.9 to estimate the range of t_f. As shown in Fig. 10, regardless of the texture geometry, there is a fair agreement between the predictions and

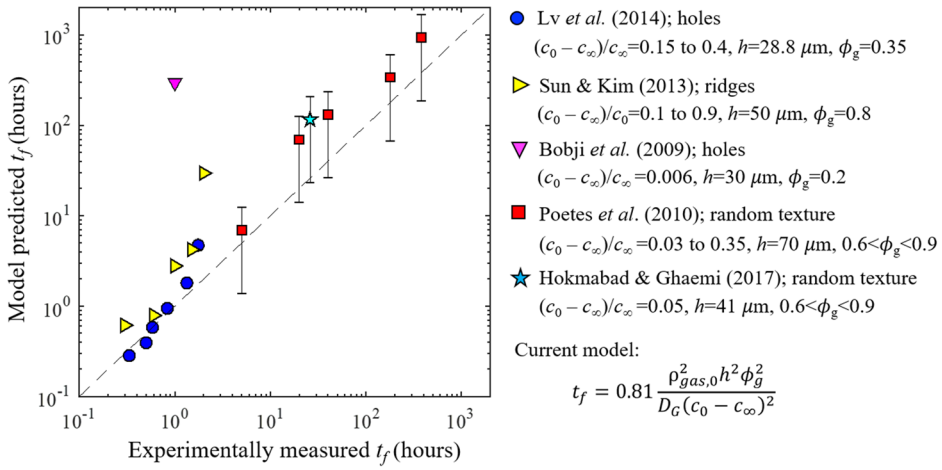

Fig. 9 A comparison between experimentally measured plastron lifetime and the predicted plastron lifetime

measurements for most cases. The mismatch between prediction and measurement could attribute to the measurement uncertainty, irregular textures, and interface instabilities in experiments [45]. In particular, the measurement based on light reflected from the SHS [41,43,60] may underestimate t_f, since light reflected from a curved or depined interface may not be detectable by the sensor. Interface instability caused by surface energy minimization could trigger a sudden collapse of the plastron [45].

The diffusion length model in Eq. (18) explains how L_D varies with the degree of under-saturation and the texture parameters. First, the model predicts that L_D reduces when increasing the degree of under-saturation. This is expected since as increasing $c_0 - c_\infty$, per amount of liquid can absorb more gas, less liquid will be impacted by the plastron, so that the gas propagates for a shorter distance. Second, our model predicts that L_D increases with increasing the texture height and the gas fraction. This is also expected since as increasing texture height or gas fraction, the amount of gas in the plastron increases, more liquid is required to absorb all the gas, so that the gas propagates for a larger distance. For the experimental conditions in Lv et al. [45], the model predicts an L_D varying from 400 to 1800 μm depending on the pressure, which is close to their reported $L_D = 450$ μm. For the experimental conditions in Kim and Park [52], L_D predicted by our model is two orders of magnitude larger than the measured 4–6 μm. This disagreement is probably because the wetting transition observed in their experiments was impacted not only by the gas diffusion but also by the interface instability induced by surface energy minimization. In fact, for the SHS used by Kim & Park, the Cassie-Baxter state has higher interfacial energy than the Wenzel state and is thus not thermodynamically stable [66].

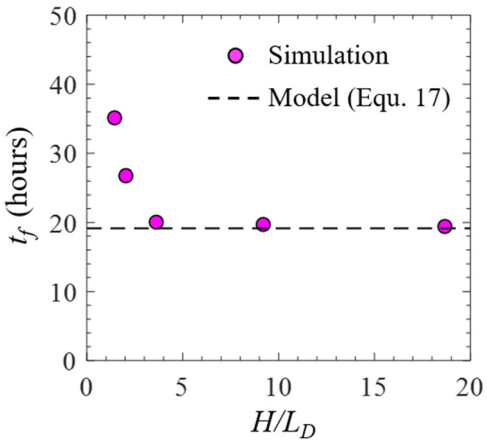

Fig. 10 Impact of the height of water tank on the plastron lifetime. In these simulations, H varies from 10 to 100 mm, and the groove dimensions are fixed (λ = 0.1 mm, w/λ = 0.5, h/λ = 1, θ_{adv} = 120 deg).

Note, in the current study, H is sufficiently large so that all gas in the plastron is dissolved in the liquid. However, when reducing H, the liquid could be fully saturated before the gas is completely dissolved, and the plastron lifetime can be infinite [40]. We expect that the proposed model of plastron lifetime holds true as long as H is sufficiently larger than L_D so that the gas concentration in the .far-field is not affected by the plastron. To examine the limit of H, we performed simulations where H varies from 10 to 100 mm, and the groove dimensions are fixed ($\lambda = 0.1$ mm, $w/\lambda = 0.5$, $h/\lambda = 1$). Figure 11 shows t_f as a function of H/L_D. As expected, for $H > 3L_D$, the model predicts the plastron lifetime very well, and the plastron lifetime does not change with H. But when $H < 3L_D$, the model under-estimates the plastron lifetime. The limit where the proposed model is valid is $H > 3L_D$ (L_D can be predicted by Eq. (18)).

4 Conclusions

In this work, we performed a numerical study of the longevity of super-hydrophobic surfaces fully submerged in under-saturated liquid. We numerically solved the spatial and temporal variations of the dissolved gas concentration in the liquid as it slowly increases during the wetting process. Based on the resolved gas concentrations and Fick's first law, we calculated the rate of mass transfer, the time-variation of the mass remaining in the plastron, and the time required for all gas to be dissolved (i.e., the plastron lifetime). We found that the gas concentration profiles at different times display a self-similarity, and the mass flux reduces with time (t) at a rate of $1/t^{0.5}$. These observations agree with the one-dimensional gas diffusion and could be attributed to the small texture size compared to the diffusion length.

Furthermore, we performed a series of numerical simulations to examine the impacts of texture parameters, including pitch, gas fraction, texture height, and advancing contact angle, on the mass flux, plastron lifetime, and diffusion length. Based on the simulation results, we proposed simple analytical model for the plastron lifetime, which does not require a per-knowledge of diffusion length or invasion coefficient. Our model showed that the SHS longevity increases with increasing the gas fraction or increasing the texture height and is independent of the advancing contact angle and texture pitch. We found that the proposed model agrees fairly well with the experimental data reported in the literature, and can predict the longevity of SHS with various texture sizes, texture geometries, and under different degrees of under-

saturations. We also proposed an analytical model for the diffusion length, which showed that the diffusion length increases with decreasing the degree of under-saturation, increasing gas fraction, or increasing the texture height. We believe our work can provide a general guideline for designing SHS with extended lifetimes when submerged in under-saturated liquid.

It should be noted that the proposed models and conclusions in this study only apply to these wetting processes which mainly consist of the depining impalement, not the sagging. These wetting processes are often observed when the pressure above the surface is larger than the critical pressure for interface to depin from the tip of texture. If the sagging stage is mainly involved, the effect of surface tension needs to be accounted. As interface curvature increases during the sagging, the gas pressure in the plastron reduces due to the surface tension, which could result in a lower mass flux. Although ignoring the sagging, the proposed model could provide a good approximation for the longevity of these SHSs which have a large ratio of texture height to width.

Acknowledgment

We thank the support by UMass Dartmouth's Marine and Undersea Technology (MUST) Research Program funded by the Office of Naval Research (ONR) under Grant No. N00014-20-1-2170. We also thank the support by National Science Foundation (NSF) under Grant No. 2041479.

Funding Data

- Office of Naval Research (ONR) (Grant No. N00014-20-1-2170; Funder ID: 10.13039/100000006).
- National Science Foundation (NSF) (Grant No. 2041479; Funder ID: 10.13039/100000001).

Nomenclature

A = area of gas-liquid interface per unit depth into the page
c = gas concentration in the liquid
c_∞ = initial gas concentration in the liquid
c_0 = initial gas concentration in the plastron
c^{1D} = gas concentration in the liquid for one-dimensional gas diffusion
D_G = diffusion coefficient
G = A non-dimensional parameter depending on SHS texture parameters
h = groove height of the SHS texture
H = height of the water column above the SHS
I = all variables should appear in italics
J_{ave} = time-average mass flux
J_{out} = mass flux averaged over gas-liquid interface
J_{out}^{1D} = mass flux averaged over gas-liquid interface for 1D gas diffusion
L_D = diffusion length scale
L_D^{1D} = diffusion length scale for 1D gas diffusion
m = mass of gas in the plastron
P_L = pressure in the water above the SHS
S = gas-liquid interface
t = time
t_D = characterize time for a SHS in under-saturated liquid
t_f = time when the mass in the plastron reduces to zero (plastron lifetime)
t_f^{1D} = plastron lifetime for 1D gas diffusion
w = groove width of the SHS texture
x = Cartesian coordinate, direction parallel to the SHS
y = Cartesian coordinate, direction normal to the SHS
λ = groove pitch of the SHS texture
$\rho_{gas,0}$ = density of gas evaluated at atmosphere pressure
θ_{adv} = advancing contact angle of the SHS
ϕ_g = fraction of surface area covered by gas on the SHS (gas fraction)

Reference

[1] Cassie, A. B. D., and Baxter, S., 1944, "Wettability of Porous Surfaces," Trans. Faraday Soc., **40**, pp. 546–551.
[2] Hwang, G. B., Page, K., Patir, A., Nair, S. P., Allan, E., and Parkin, I. P., 2018, "The Anti-Biofouling Properties of Superhydrophobic Surfaces Are Short-Lived," ACS Nano, **12**(6), pp. 6050–6058.
[3] Mohamed, A. M. A., Abdullah, A. M., and Younan, N. A., 2015, "Corrosion Behavior of Superhydrophobic Surfaces: A Review," Arab. J. Chem., **8**(6), pp. 749–765.
[4] Lee, C., Choi, C. H., and Kim, C. J., 2016, "Superhydrophobic Drag Reduction in Laminar Flows: A Critical Review," Exp. Fluids, **57**(12), pp. 1–20.
[5] Ou, J., Perot, B., and Rothstein, J. P., 2004, "Laminar Drag Reduction in Microchannels Using Ultrahydrophobic Surfaces," Phys. Fluids, **16**(12), pp. 4635–4643.
[6] Choi, C. H., and Kim, C. J., 2006, "Large Slip of Aqueous Liquid Flow Over a Nanoengineered Superhydrophobic Surface," Phys. Rev. Lett., **96**(6), pp. 1–4.
[7] Ybert, C., Barentin, C., Cottin-Bizonne, C., Joseph, P., and Bocquet, L., 2007, "Achieving Large Slip With Superhydrophobic Surfaces: Scaling Laws for Generic Geometries," Phys. Fluids, **19**(12), p. 123601.
[8] Lee, C., Choi, C.-H., and Kim, C.-J., 2008, "Structured Surfaces for a Giant Liquid Slip," Phys. Rev. Lett., **101**(6), p. 064501.
[9] Rothstein, J. P., 2010, "Slip on Superhydrophobic Surfaces," Annu. Rev. Fluid Mech., **42**(1), pp. 89–109.
[10] Woolford, B., Prince, J., Maynes, D., and Webb, B. W., 2009, "Particle Image Velocimetry Characterization of Turbulent Channel Flow With Rib Patterned Superhydrophobic Walls," Phys. Fluids, **21**(8), p. 085106.
[11] Daniello, R. J., Waterhouse, N. E., and Rothstein, J. P., 2009, "Drag Reduction in Turbulent Flows Over Superhydrophobic Surfaces," Phys. Fluids, **21**(8), p. 085103.
[12] Bidkar, R. A., Leblanc, L., Kulkarni, A. J., Bahadur, V., Ceccio, S. L., and Perlin, M., 2014, "Skin-Friction Drag Reduction in the Turbulent Regime Using Random-Textured Hydrophobic Surfaces," Phys. Fluids, **26**(8), p. 085108.
[13] Park, H., Sun, G., and Kim, C.-J., 2014, "Superhydrophobic Turbulent Drag Reduction as a Function of Surface Grating Parameters," J. Fluid Mech., **747**, pp. 722–734.
[14] Ling, H., Srinivasan, S., Golovin, K., McKinley, G. H., Tuteja, A., and Katz, J., 2016, "High-Resolution Velocity Measurement in the Inner Part of Turbulent Boundary Layers Over Super-Hydrophobic Surfaces," J. Fluid Mech., **801**, pp. 670–703.
[15] Gose, J. W., Golovin, K., Boban, M., Mabry, J. M., Tuteja, A., Perlin, M., and Ceccio, S. L., 2018, "Characterization of Superhydrophobic Surfaces for Drag Reduction in Turbulent Flow," J. Fluid Mech., **845**, pp. 560–580.
[16] Reholon, D., and Ghaemi, S., 2018, "Plastron Morphology and Drag of a Superhydrophobic Surface in Turbulent Regime," Phys. Rev. Fluids, **3**(10), pp. 1–21.
[17] Rajappan, A., Golovin, K., Tobelmann, B., Pillutla, V., Abhijeet, Tuteja, A., and McKinley, G. H., 2019, "Influence of Textural Statistics on Drag Reduction by Scalable, Randomly Rough Superhydrophobic Surfaces in Turbulent Flow," Phys. Fluids, **31**(4), p. 042107.
[18] Xu, M., Yu, N., Kim, J. J., and Kim, C.-J., 2021, "Superhydrophobic Drag Reduction in High-Speed Towing Tank," J. Fluid Mech., **908**, p. A6.
[19] Mehanna, Y. A., Sadler, E., Upton, R. L., Kempchinsky, A. G., Lu, Y., and Crick, C. R., 2021, "The Challenges, Achievements and Applications of Submersible Superhydrophobic Materials," Chem. Soc. Rev., **50**(11), pp. 6569–6612.
[20] Wenzel, R. N., 1936, "Resistance of Solid Surfaces to Wetting by Water," Ind. Eng. Chem., **28**(8), pp. 988–994.
[21] Vajdi Hokmabad, B., and Ghaemi, S., 2016, "Turbulent Flow Over Wetted and Non-Wetted Superhydrophobic Counterparts With Random Structure," Phys. Fluids, **28**(1), p. 015112.
[22] Zheng, Q.-S., Yu, Y., and Zhao, Z.-H., 2005, "Effects of Hydraulic Pressure on the Stability and Transition of Wetting Modes of Superhydrophobic Surfaces," Langmuir, **21**(26), pp. 12207–12212.
[23] Papadopoulos, P., Mammen, L., Deng, X., Vollmer, D., and Butt, H.-J., 2013, "How Superhydrophobicity Breaks Down," Proc. Natl. Acad. Sci., **110**(9), pp. 3254–3258.
[24] Extrand, C. W., 2011, "Repellency of the Lotus Leaf: Resistance to Water Intrusion Under Hydrostatic Pressure," Langmuir, **27**(11), pp. 6920–6925.
[25] Seo, J., García-Mayoral, R., and Mani, A., 2015, "Pressure Fluctuations and Interfacial Robustness in Turbulent Flows Over Superhydrophobic Surfaces," J. Fluid Mech., **783**, pp. 448–473.
[26] Seo, J., and Mani, A., 2018, "Effect of Texture Randomization on the Slip and Interfacial Robustness in Turbulent Flows Over Superhydrophobic Surfaces," Phys. Rev. Fluids, **3**(4), pp. 1–15.
[27] Rastegari, A., and Akhavan, R., 2019, "On Drag Reduction Scaling and Sustainability Bounds of Superhydrophobic Surfaces in High Reynolds Number Turbulent Flows," J. Fluid Mech., **864**, pp. 327–347.
[28] Seo, J., García-Mayoral, R., and Mani, A., 2018, "Turbulent Flows Over Superhydrophobic Surfaces: Flow-Induced Capillary Waves, and Robustness of Air-Water Interfaces," J. Fluid Mech., **835**, pp. 45–85.
[29] Cartagena, E. J. G., Arenas, I., Bernardini, M., and Leonardi, S., 2018, "Dependence of the Drag Over Super Hydrophobic and Liquid Infused Surfaces on the Textured Surface and Weber Number," Flow Turbul. Combust., **100**(4), pp. 945–960.
[30] Hyväluoma, J., and Harting, J., 2008, "Slip Flow Over Structured Surfaces With Entrapped Microbubbles," Phys. Rev. Lett., **100**(24), p. 246001.

[31] Gao, P., and Feng, J. J., 2009, "Enhanced Slip on a Patterned Substrate Due to Depinning of Contact Line," Phys. Fluids, **21**(10), p. 102102.
[32] Huang, S., Lv, P., and Duan, H., 2019, "Morphology Evolution of Liquid–Gas Interface on Submerged Solid Structured Surfaces," Extrem. Mech. Lett., **27**, pp. 34–51.
[33] Xue, Y., Lv, P., Lin, H., and Duan, H., 2016, "Underwater Superhydrophobicity: Stability, Design and Regulation, and Applications," ASME Appl. Mech. Rev., **68**(3), p. 030803.
[34] Emami, B., Hemeda, A. A., Amrei, M. M., Luzar, A., Gad-el-Hak, M., and Vahedi Tafreshi, H., 2013, "Predicting Longevity of Submerged Superhydrophobic Surfaces With Parallel Grooves," Phys. Fluids, **25**(6), p. 062108.
[35] Hemeda, A. A., Gad-el-Hak, M., and Tafreshi, H. V., 2014, "Effects of Hierarchical Features on Longevity of Submerged Superhydrophobic Surfaces With Parallel Grooves," Phys. Fluids, **26**(8), p. 082103.
[36] Piao, L., and Park, H., 2015, "Two-Dimensional Analysis of Air-Water Interface on Superhydrophobic Grooves Under Fluctuating Water Pressure," Langmuir, **31**(29), pp. 8022–8032.
[37] Hemeda, A. A., and Vahedi Tafreshi, H., 2015, "Instantaneous Slip Length in Superhydrophobic Microchannels Having Grooves With Curved or Dissimilar Walls," Phys. Fluids, **27**(10), p. 102101.
[38] Hemeda, A. A., and Tafreshi, H. V., 2014, "General Formulations for Predicting Longevity of Submerged Superhydrophobic Surfaces Composed of Pores or Posts," Langmuir, **30**(34), pp. 10317–10327.
[39] Flynn, M. R., and Bush, J. W. M., 2008, "Underwater Breathing: The Mechanics of Plastron Respiration," J. Fluid Mech., **608**, pp. 275–296.
[40] Kadoko, J., Karamanis, G., Kirk, T., and Hodes, M., 2017, "One-Dimensional Analysis of Gas Diffusion-Induced Cassie to Wenzel State Transition," ASME J. Heat Transfer-Trans. ASME, **139**(12), pp. 1–10.
[41] Bobji, M. S., Kumar, S. V., Asthana, A., and Govardhan, R. N., 2009, "Underwater Sustainability of the 'Cassie' State of Wetting," Langmuir, **25**(20), pp. 12120–12126.
[42] Govardhan, R. N., Srinivas, G. S., Asthana, A., and Bobji, M. S., 2009, "Time Dependence of Effective Slip on Textured Hydrophobic Surfaces," Phys. Fluids, **21**(5), p. 052001.
[43] Poetes, R., Holtzmann, K., Franze, K., and Steiner, U., 2010, "Metastable Underwater Superhydrophobicity," Phys. Rev. Lett., **105**(16), p. 166104.
[44] Samaha, M. A., Vahedi Tafreshi, H., and Gad-el-Hak, M., 2012, "Sustainability of Superhydrophobicity Under Pressure," Phys. Fluids, **24**(11), p. 112103.
[45] Lv, P., Xue, Y., Shi, Y., Lin, H., and Duan, H., 2014, "Metastable States and Wetting Transition of Submerged Superhydrophobic Structures," Phys. Rev. Lett., **112**(19), p. 196101.
[46] Li, X., Wang, Y., Zeng, B., Li, Y., Tan, H., Zandvliet, H. J. W., Zhang, X., and Lohse, D., 2018, "Entrapment and Dissolution of Microbubbles Inside Microwells," Langmuir, **34**(36), pp. 10659–10667.
[47] Arunachalam, S., Ahmad, Z., Das, R., and Mishra, H., 2020, "Counterintuitive Wetting Transitions in Doubly Reentrant Cavities as a Function of Surface Make-Up, Hydrostatic Pressure, and Cavity Aspect Ratio," Adv. Mater. Interfaces, **7**(22), p. 2001268.
[48] Checco, A., Ocko, B. M., Rahman, A., Black, C. T., Tasinkevych, M., Giacomello, A., and Dietrich, S., 2014, "Collapse and Reversibility of the Superhydrophobic State on Nanotextured Surfaces," Phys. Rev. Lett., **112**(21), pp. 1–5.
[49] Xu, M., Sun, G., and Kim, C.-J., 2014, "Infinite Lifetime of Underwater Superhydrophobic States," Phys. Rev. Lett., **113**(13), p. 136103.
[50] Sun, W.-Y., and Kim, C.-J. C. J., 2013, "The Role of Dissolved Gas in Longevity of Cassie States for Immersed Superhydrophobic Surfaces," IEEE 26th International Conference on Micro Electro Mechanical Systems (MEMS), IEEE, Taipei, Taiwan, Jan. 20–24, pp. 397–400.
[51] Patankar, N. A., 2016, "Thermodynamics of Trapping Gases for Underwater Superhydrophobicity," Langmuir, **32**(27), pp. 7023–7028.
[52] Kim, H., and Park, H., 2019, "Diffusion Characteristics of Air Pockets on Hydrophobic Surfaces in Channel Flow: Three-Dimensional Measurement of Air-Water Interface," Phys. Rev. Fluids, **4**(7), p. 074001.
[53] Karatay, E., Tsai, P. A., and Lammertink, R. G. H., 2013, "Rate of Gas Absorption on a Slippery Bubble Mattress," Soft Matter, **9**(46), pp. 11098–11106.
[54] Haase, A. S., Karatay, E., Tsai, P. A., and Lammertink, R. G. H., 2013, "Momentum and Mass Transport Over a Bubble Mattress: The Influence of Interface Geometry," Soft Matter, **9**(37), p. 8949.
[55] Chellam, S., Wiesner, M. R., and Dawson, C., 1992, "Slip at a Uniformly Porous Boundary: Effect on Fluid Flow and Mass Transfer," J. Eng. Math., **26**(4), pp. 481–492.
[56] Barth, C., Samaha, M., Tafreshi, H., and Gad-el-Hak, M., 2013, "Convective Mass Transfer From Submerged Superhydrophobic Surfaces," Int. J. Flow Control, **5**(2), pp. 79–88.
[57] Barth, C., Samaha, M., Tafreshi, H., and Gad-el-Hak, M., 2013, "Convective Mass Transfer From Submerged Superhydrophobic Surfaces: Turbulent Flow," Int. J. Flow Control, **5**(3–4), pp. 143–152.
[58] Dilip, D., Jha, N. K., Govardhan, R. N., and Bobji, M. S., 2014, "Controlling Air Solubility to Maintain 'Cassie' State for Sustained Drag Reduction," Colloids Surf. A Physicochem. Eng. Asp., **459**, pp. 217–224.
[59] Dilip, D., Bobji, M. S., and Govardhan, R. N., 2015, "Effect of Absolute Pressure on Flow Through a Textured Hydrophobic Microchannel," Microfluid. Nanofluid., **19**(6), pp. 1409–1427.
[60] Hokmabad, B. V., and Ghaemi, S., 2017, "Effect of Flow and Particle-Plastron Collision on the Longevity of Superhydrophobicity," Sci. Rep., **7**(1), p. 41448.
[61] Samaha, M. A., Tafreshi, H. V., and Gad-El-Hak, M., 2012, "Influence of Flow on Longevity of Superhydrophobic Coatings," Langmuir, **28**(25), pp. 9759–9766.
[62] Xiang, Y., Xue, Y., Lv, P., Li, D., and Duan, H., 2016, "Influence of Fluid Flow on the Stability and Wetting Transition of Submerged Superhydrophobic Surfaces," Soft Matter, **12**(18), pp. 4241–4246.
[63] Ling, H., Katz, J., Fu, M., and Hultmark, M., 2017, "Effect of Reynolds Number and Saturation Level on Gas Diffusion in and Out of a Superhydrophobic Surface," Phys. Rev. Fluids, **2**(12), p. 124005.
[64] Tuteja, A., Choi, W., Ma, M., Mabry, J. M., Mazzella, S. A., Rutledge, G. C., McKinley, G. H., and Cohen, R. E., 2007, "Designing Superoleophobic Surfaces," Science (80-.), **318**(5856), pp. 1618–1622.
[65] Xue, Y., Chu, S., Lv, P., and Duan, H., 2012, "Importance of Hierarchical Structures in Wetting Stability on Submersed Superhydrophobic Surfaces," Langmuir, **28**(25), pp. 9440–9450.
[66] Patankar, N. A., 2004, "Transition Between Superhydrophobic States on Rough Surfaces," Langmuir, **20**(17), pp. 7097–7102.